Proceedings of the 15th International Pipeline Conference 2020
IPC2020
September 28-October 02, 2020, Calgary, Alberta, Canada

IPC2020-14253

PIPELINE FRACTURE CONTROL CONCEPTS FOR NORWEGIAN OFFSHORE CARBON CAPTURE AND STORAGE

Gaute Gruben[1], Kenneth Macdonald[2], Svend T. Munkejord[3], Hans L. Skarsvåg[3] and Stephane Dumoulin[1]

[1]SINTEF Industry, Trondheim, Norway
[2]Equinor/University of Stavanger, Stavanger, Norway
[3]SINTEF Energy Research, Trondheim, Norway

ABSTRACT

The Northern Lights onshore terminal will initially receive CO_2 transported by ship tankers from industrial source sites located in south-eastern Norway and transport CO_2 via a 12 ¾" OD offshore pipeline for injection into the Johansen storage reservoir, located south of the Troll field. The CO_2 injection pipeline will be laid from the shore terminal to a subsea wellhead structure from where the liquid CO_2 will be injected into the reservoir. Presently, demonstrating arrest of longitudinal propagating shear fracture in CO_2 transport pipelines is specifically addressed in two international guidelines, ISO 27913 and DNVGL-RP-F104. The study reported here aims to develop a robust fracture control methodology unique to the Northern Lights pipeline. To this end, the maximum loading in terms of saturation pressure is conservatively estimated from temperature and pressure scenarios from the planned pipeline route and applied in numerical simulations of the running-fracture phenomenon using the SINTEF coupled FE-CFD code. It is shown that, with the given pipe material, diameter, and loading conditions, the proposed wall thickness of 15.9 mm is sufficient to arrest a propagating crack. Furthermore, the Battelle TCM with ISO 27913 or DNVGL-RP-F104 arrest- and load pressure correction is shown to provide a good first estimate in pipe design, although the arrest pressure saturates for low Charpy energy toughness values, indicating limited accuracy in this study.

Keywords: Pipeline design, running ductile fracture, CO_2 transport

1. INTRODUCTION

The Northern Lights onshore terminal will receive CO_2 transported by tankers from industrial source sites located in south-eastern Norway, temporarily store liquid CO_2 onshore in tanks at the terminal, and finally transport CO_2 via a 12 ¾" OD offshore pipeline for injection into the Johansen storage reservoir, located south of the Troll field. The full-scale CCS concept is illustrated in FIGURE 1. The CO_2 injection pipeline will be laid to a subsea structure where the fluid will be injected. The pipeline is sized for the transport volumes from the CO_2 capture sites under the existing contract with Gassnova, but with additional capacity to accommodate defined future volumes.

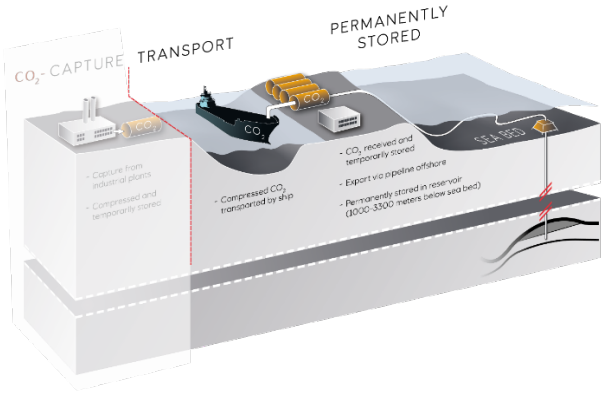

FIGURE 1: NORTHERN LIGHTS CO_2 TRANSPORT AND STORAGE CHAIN

Arrest of running-ductile fractures (longitudinal shear) is a long-established design aspect of pipeline systems transmitting hydrocarbon gas. Research on this topic at the Battelle Memorial Institute in the 1960s and 70s, culminated in the Two Curve Method (TCM) [1]. Here, a semi-empirical curve with the crack velocity expressed as a function of pressure is compared with the decompression velocity curve of the gas, and the rationale is that the crack arrests if the velocity of the decompression curve is higher than the crack velocity for all pressure values.

In a running-ductile fracture, the crack-driving force stems from the fluid pressure on the pipe walls downstream of the crack-tip. It follows that a larger pipe diameter gives a larger area for the pressure to work on and therefore a larger crack-driving force. In the event of a sudden opening in a pressurized pipeline, the fluid will escape from the opening while decompressing along the pipeline [1]. If the fluid is in the liquid state before and

after decompression which, for example, is the case for water and oil, the pressure near the crack drops rapidly due to the large decompression velocity, and no significant crack-driving force will be present to propagate the crack [2]. In pipelines where the fluid is in the gas phase before and after decompression (e.g. lean gas), and in particular, where the fluid enters a two-phase state during decompression (e.g. rich natural gas), there is a risk that the propagating crack will run at a higher velocity due to a higher pressure at and downstream of the crack-tip, which again is related to the decompression velocity of the fluid. In a (dense) liquid CO_2 pipeline, the primary decompression wave runs through the liquid at a velocity which is typically higher than that of a running-ductile fracture. However, behind the primary decompression wave, boiling CO_2 prevails at high pressure. Thus, the crack-driving force in a CO_2 pipeline stems from the boiling pressure and does not directly depend on the velocity of the primary decompression wave. Maxey addressed this phenomenon [3] and suggested that the TCM in this case should be applied such that crack arrest is predicted if the (velocity independent) arrest pressure of the pipe is higher than the boiling pressure of the CO_2, i.e. the two curves in the TCM are replaced by two single values: the arrest pressure and the saturation pressure. This two-point application of the TCM for CO_2 pipelines has been implemented in international design guidelines [4, 5]. Recent experimental studies [6-9] have shown that direct application of the two-point TCM on CO_2 pipelines is non-conservative and that additional factors are needed. Although securing adequate fracture toughness in the line pipe steel (and defining what level is adequate by analysis or testing) is the primary mitigation strategy to quickly arrest running-ductile fracture, alternative methods such as crack arrestors at intermediate locations may be used to address particularly challenging circumstances. Dense-phase CO_2 has similar decompression characteristics to those of rich natural gas, so the same general design challenge also exists for these pipelines. The challenge lies in determining the applicability of the existing industry-standard assessment methods for natural gas to CO_2-transport pipeline systems.

DNVGL-RP-F104 [4] and ISO 27913 [5] both open for use of numerical methods in design of CO_2 pipelines. The former guideline states that 'A numerical model for prediction of the decompression of outflow behavior must be capable to deal with a high transient flow and therefore requires tracking of the expansion wave and the propagation as function of time and distance along the pipeline length.' Several studies of numerical approaches for predicting crack propagation/arrest have been conducted, e.g. [10-13]. However, studies where multi-phase CO_2 is the loading medium are scarce. Mahgerefeteh et al. [14] used a simplified structural mechanics approach in making fracture predictions of CO_2 pipelines, while recently, Keim and coworkers [15, 16] presented an advanced steel material model applied in combination with modelling of the CO_2 and the backfill. In the present study, the SINTEF FE-CFD code is applied. Here, a computational fluid dynamics (CFD) solver is coupled to a finite element (FE) solver by a user defined load routine. This provides full coupling in the numerical calculations of the steel pipe with the propagating crack and the fluid decompression. The FE-CFD code has previously been compared with experimental burst data with CO_2 as a loading medium [17-19].

2. DESIGN BASIS

Three alternative pipeline routes were considered at the front-end engineering phase as shown in FIGURE 2. All of them led to a pipeline of approximately 70 km length with an onshore part of maximum 10 km. The storage reservoir has been subsequently changed but, as will be shown, this does not influence the conclusions from the present study. The temperature along the pipeline for liquid CO_2 based on maximum, mean and minimum ambient temperature is estimated for low, medium and high flowrates as shown in FIGURE 3. Here, the peak temperature in the maximum ambient temperature case (19 °C) occurs in the low flowrate case in shallow water near the onshore facility. For any flow rate, the temperature converges to 10 °C in the submerged pipeline in the maximum ambient temperature case. The design operation pressure was established as 250 bar at 30 m above mean sea level in the front-end engineering phase. Typical pressure profiles for the pipeline are shown in FIGURE 4. These profiles are given based on an assumed wellhead pressure of 75 bar, which is the minimum wellhead pressure to secure single-phase liquidin the pipeline. Note that the wellhead pressure may also be higher depending on the reservoir pressure and the frictional pressure loss in the well. Since the transport of the CO_2 to the onshore terminal is by containers and in the liquid state, the CO_2 can be considered free of impurities capable of increasing the boiling pressure.

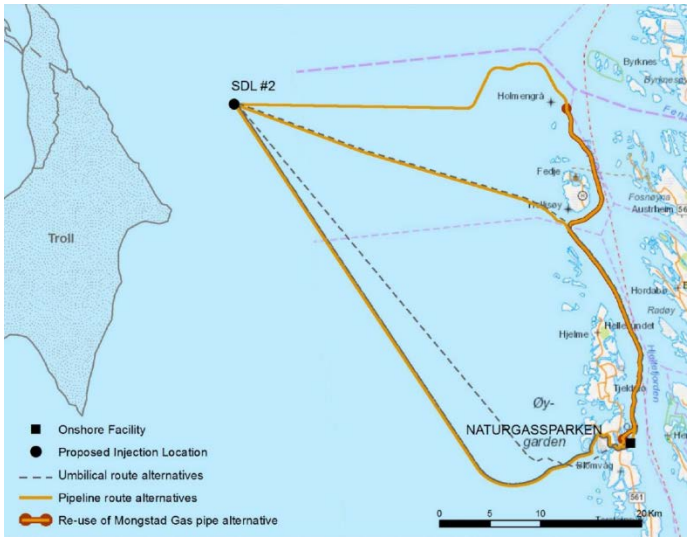

FIGURE 2: THREE ALTERNATIVE PIPELINE ROUTES AT THE TIME OF DESIGN FOR RUNNING FRACTURE

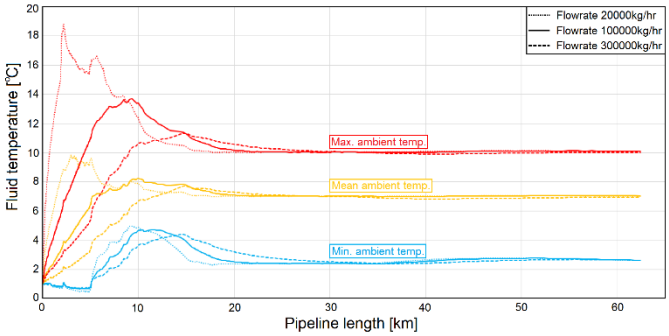

FIGURE 3: TEMPERATURE PROFILES FOR LOW (20000 kg/hr), MEDIUM (100000 kg/hr) AND HIGH (300000 kg/hr) FLOWRATES FOR MAXIMUM, MEAN AND MINIMUM AMBIENT TEMPERATURE

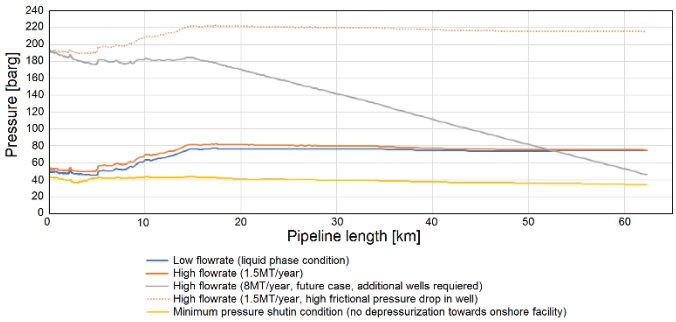

FIGURE 4: PRESSURE PROFILE FOR VARIOUS FLOWRATES AND FOR SHUTIN CONDITION

The base-case dimensions of the pipe were originally selected to match the Mongstad Gas Pipeline, which was an early re-use candidate, see FIGURE 2. The input parameters for the onshore and offshore pipeline are identical. The pipeline is of grade DNVGL 450 (X65) and the geometry is based in part on reel-installation. Both seamless and HFW pipes are considered, although it is stated that an HFW line pipe may be an economic upside for the project. The parameters are summarized below.

- Outer diameter, OD: 323.9 mm
- Wall thickness, *t*: 15.9 mm or 17.5 mm. 15.9 mm is used for running ductile fracture design
- Fabrication wall thickness tolerance: ±10 %
- Specified minimum yield stress at 20 °C: 450 MPa
- Specified minimum tensile strength at 20 °C: 535 MPa
- Maximum allowable yield to tensile ratio: 0.92
- Material (hardening) strength factor: 0.96
- Young's modulus: 207 GPa
- Poisson's ratio: 0.3
- Steel density: 7850 kg/m
- Charpy V-notch (CVN) value: minimum specified 125 J, actual 200-450 J. Design is to be conducted for 100 J, 125 J and 200 J.
- Drop Weight Tear Test (DWTT) requirement: 85 % shear area at minimum operating temperature
- Out-of-roundness: 1.5 %
- Girth weld factor: 0.996

3. ESTIMATE OF LOADING CONDITIONS

Should there be a leak from a large hole in the pipe, the pressure in the liquid CO_2 is rapidly reduced. The expansion of the fluid also leads to a reduced temperature. At a certain pressure, gas starts forming, i.e. we have a boiling fluid. For thermodynamic equilibrium, this pressure is known as the saturation pressure, and is a function of the fluid temperature, see the blue dashed line in FIGURE 5. The saturation pressure is a key parameter in the analysis that follows. It is therefore important to accurately model the depressurization process to determine the saturation pressure from the initial state, prior to the pipe fracture. To model the thermodynamic properties of CO_2, we employ the highly accurate reference equation of state (EOS) of Span and Wagner [20].

Rapid depressurization is an isentropic process. By calculating the entropy of the initial state, we map the temperature and pressure until the saturation pressure is reached. In FIGURE 5 we give five load cases for illustration. Load case I is based on the peak fluid temperature (19 °C) for maximum ambient temperature and a low onshore operational pressure (57 bar). This load case has a saturation pressure of 55.8 bar and can be considered as very conservative due to the low operational pressure (as will be discussed below) and that this load case is present for a limited part of the pipeline for a very limited time-period each year. The effect of initial temperature is clear when considering the saturation pressure, i.e. the blue dashed line in FIGURE 5: higher initial temperature gives higher saturation pressure. Load case II with 10 °C fluid temperature has the minimum onshore operational pressure (47 bar) to maintain single-phase flow at the well head. It can be seen from FIGURE 5 that case II has a saturation pressure that is ~11 bar lower than case I due to the 9 °C reduction in initial temperature. Load case III has the same initial temperature as load case II but is given an increase in operational CO_2 pressure (28 bar) equal to what can be expected 300 m below sea level. The higher operational pressure leads to a reduction of saturation pressure of ~3 bar. Load case IV is also similar to load case II, but here the operational pressure is set to 190 bar. This gives a saturation pressure that is lowered by ~11 bar. The influence of the operational pressure is clear: increased initial pressure gives lower saturation pressure. A conservative estimate of the maximum loading for the pipeline is thus associated with load case I, which is characterized by low initial pressure and high temperature that can occur at the landfall near the onshore facility over a short period during summer. A more realistic onshore loading in a running ductile fracture event is a saturation pressure less than 30 bar, based on an operational pressure of 250 bar and a temperature of 7 °C. For comparison, the maximum saturation pressure for pure CO_2 is 73.8 bar illustrated as load case V in FIGURE 5.

Another important aspect of the loading condition is that the effective load stems from the pressure differential over the pipe wall. In a submerged pipeline at 300 m depth, the pressure on the outer pipe wall is increased by 30.1 bar. This means that in load case III the effective loading is only 11.5 bar. Thus, it can be concluded that the larger part of the pipeline, that is submerged to more than 100 m, is significantly less susceptible to running-ductile fracture than the onshore and landfall sections.

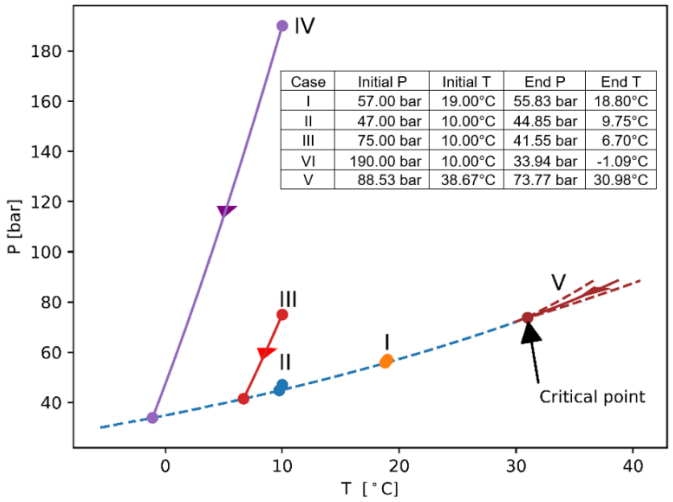

Case	Initial P	Initial T	End P	End T
I	57.00 bar	19.00°C	55.83 bar	18.80°C
II	47.00 bar	10.00°C	44.85 bar	9.75°C
III	75.00 bar	10.00°C	41.55 bar	6.70°C
VI	190.00 bar	10.00°C	33.94 bar	-1.09°C
V	88.53 bar	38.67°C	73.77 bar	30.98°C

FIGURE 5: ILLUSTRATION OF THE SATURATION PRESSURE (BLUE DASHED LINE) AND 5 LOAD CASES

4. TCM ANALYSES

4.1 Analysis for CO_2 pipelines

Traditionally, the TCM is applied to estimate the material's Charpy V-notch (CVN) energy requirement to arrest a running fracture. The TCM is based on the Dugdale fracture model, the ideal gas law and empirical data from a large campaign of burst tests [1]. As pointed out in the introduction, the 'two-curve-method' for CO_2 reduces to a 'two-scalar-method' [3]. This means that the saturation pressure is compared with the pipe's ability to withstand a propagating crack under static conditions. The condition for crack arrest for a CO_2 pipeline is then expressed as

$$p_s \le p_a \tag{1}$$

where p_s is the saturation pressure and p_a is the arrest pressure. The arrest pressure is related to the critical hoop stress, σ_a, such that $\sigma_a = p_a R/t$, where R is the pipe radius and t is the wall thickness. Following the TCM, the pipe's critical hoop stress for static conditions is expressed by [1]:

$$\frac{C_V E}{A_c \sigma_f^2 \sqrt{Rt}} = \frac{24}{\pi} \ln\left(\sec\left(\frac{\pi}{2}\frac{3.33\sigma_a}{\sigma_f}\right)\right) \tag{2}$$

where A_c is the area of the Charpy specimen, C_V is the material's CVN value, E is the material's Young modulus and σ_f is the equivalent flow stress of the pipe material. By rearranging Eq. (2), we find the arrest pressure as:

$$p_a = \frac{2\sigma_f \cdot t}{3.33\pi R} \arccos\left(\exp\left(-\frac{C_V \cdot E\pi}{24 A_c \sigma_f^2 \sqrt{Rt}}\right)\right) \tag{3}$$

4.2 Safety factors

Since the TCM has proven to be non-conservative for rich gases and CO_2 in combination with modern steels, several correction factors have been proposed [21]. One group of correction factors is applied to the predicted C_V value to arrest a running fracture for a given loading condition. Among these corrections, the Wilkowski correction [22] is considered to be the most conservative [23]. The Wilkowski correction gives a corrected CVN value as:

$$C_V^W = 0.056(0.102C_V + 10.29)^{2.597} - 16.81 \tag{4}$$

i.e. in this type of analysis $C_V^W \ge C_V$. However, in a design situation where the CVN value is known, and the arrest pressure is to be estimated from a conservative Wilkowski correction, Eq. (4) has to be rearranged so that:

$$C_V^W = \left(\left(C_V + 16.81\right)/0.056\right)^{\frac{1}{2.597}} - 10.29\Big) / 0.102 \tag{5}$$

That is, in this case, $C_V^W \le C_V$. TABLE 1 compiles the C_V^W values corresponding to the given C_V considered in this study,

TABLE 1: GIVEN AND EQ. (5) CORRECTED CHARPY V-NOTCH VALUES

C_V	100 J	125 J	200 J
C_V^W	85 J	100 J	135 J

In the procedure suggested in the appendix of ISO27913 [5], a correction factor with a recommended value $c_{cf} \ge 1.2$, should be applied to the predicted arrest pressure for all materials having a CVN value less than 330 J. This implies a modification of Eq. (3), and the ISO27913 arrest pressure, p_a^{ISO}, is expressed as:

$$p_a^{ISO} = \frac{1}{c_{cf}} \frac{2\sigma_f t}{3.33\pi R} \arccos\left(\exp\left(-\frac{C_V \cdot E\pi}{24 A_c \sigma_f^2 \sqrt{Rt}}\right)\right) \tag{6}$$

According to DNV-GL RP-F104 [4] an estimate of the saturation pressure should be performed based on a conservative CO_2 stream composition. Furthermore, a safety factor is recommended for both the saturation pressure (load factor γ_{sat}) and the arrest pressure (material factor γ_{CO2}). This leads to a modification of Eq. (1) so that the following condition must be fulfilled to avoid unstable propagation:

$$p_s \cdot \gamma_{sat} \le \frac{p_a}{\gamma_{CO2}} \tag{7}$$

DNV-GL RP-F104 does not specify any values for γ_{sat} or γ_{CO2}. Furthermore, it can be seen that γ_{CO2} can be interpreted as serving the same function as c_{cf} in ISO27913.

4.3 TCM results for the specified pipe section

Three cases with different arrest pressure calculations are performed for C_V values of 100 J, 125 J and 200 J:

1. No correction; Eq. (3) with C_V
2. Wilkowski correction; Eq. (3) with C_V^W from Eq. (5) instead of C_V
3. ISO27913 correction; Eq. (6) with C_V and $c_{cf} = 1.2$

In the TCM analyses, the σ_f value is taken as the average of SMYS and SMTS since this is more conservative than the alternative value given by SMYS+68.9 MPa. The applied input parameters are given below, and the calculated results are given in TABLE 2.

- $t = 15.9$ mm
- $E = 207$ GPa
- $R = 161.95$ mm
- $A_c = 80$ mm^2
- $\sigma_f = 492.5$ MPa
- $c_{cf} = 1.2$

TABLE 2: PREDICTED ARREST PRESSURE WITH AND WITHOUT SAFETY CORRECTION

Case	$C_V = 100$ J	$C_V = 125$ J	$C_V = 200$ J
1. No correction	140.2 bar	143.1 bar	145.7 bar
2. Wilkowski	137.2 bar	140.1 bar	143.8 bar
3. ISO27913	117.0 bar	119.4 bar	121.6 bar

From TABLE 2 it can be seen that even the most conservative estimate of the arrest pressure is larger than 117 bar. For comparison, the largest expected saturation pressure determined as load case I in Section 3 is 54.8 barg and the maximum saturation pressure for CO_2 is 72.8 barg at atmospheric pressure outside the pipe. Using the maximum saturation pressure in TCM design will correspond to a safety factor $\gamma_{sat} = 1.3$ following DNV-GL RP-F104 [4]. In a buried or submerged pipe, a higher pressure is present immediately outside the pipe, and this will add additional resistance to a running fracture. In summary, this indicates that running ductile fracture is highly unlikely to occur based on the TCM analysis. Furthermore, it can be seen that the arrest pressure increases by only ~5 bar when increasing C_V from 100 J to 200 J. This suggests that the arccos factor in Eqs. (1) and (6) has saturated already at $C_V = 100$ J. This also explains why the Wilkowski correction reduces the arrest pressure by only 3 bar or less. On the other hand, the ISO27813 correction does not saturate, since this correction is proportional to the arrest pressure. With $c_{cf} = 1.2$, the arrest pressure is reduced by approximately 24 bar. In summary, for these specific pipe data, the CVN value and the Wilkowski correction have only a minor influence on the predicted arrest pressure, whilst the ISO27813 correction gives a significantly more conservative estimate of the arrest pressure. Finally, the predicted arrest pressure is significantly higher than the maximum loading (saturation) pressure and thus the TCM analysis predicts crack arrest for this pipe under the given loading conditions.

The minimum wall thickness for the present pipe section, $t_{\min}$, to withstand a given saturation pressure, can be calculated following DNV-GL RP104 [4] procedures by applying Eq. (3) and Eq. (7). The resulting $t_{\min}$ values for a saturation pressure of $p_s = 54.8$ barg ($\gamma_{sat} = 1.0$) and $p_s = 72.8$ barg ($\gamma_{sat} = 1.3$) are shown in TABLE 3. The $t_{\min}$ values for $p_s = 54.8$ barg correspond to the minimum requirement in ISO27813 and is here 7.3 mm. The load case $p_s = 72.8$ barg gives a minimum wall thickness of ~9.6 mm. Once again, the saturated arccos factor in Eq. (3) leads to only a small variation in $t_{\min}$ for the three CVN values. In conclusion, a conservative estimate following DNV-GL RP-F104 procedures with $\gamma_{CO2} = 1.2$ and $\gamma_{sat} = 1.3$ gives a minimum wall thickness of 9.6 mm to ensure crack arrest.

TABLE 3: MINIMUM WALL THICKNESS FROM TCM ANALYSES WITH $\gamma_{sat} = 1.3$ ($p_s = 72.8$ barg), $\gamma_{sat} = 1.0$ ($p_s = 54.8$ barg) AND $\gamma_{CO2} = 1.2$. RESULTS FROM THE FE-CFD ANALYSES ARE ALSO SHOWN

	$C_V = 100$ J	$C_V = 125$ J	$C_V = 200$ J
$p_s = 72.8$ barg	9.6 mm	9.5 mm	9.5 mm
$p_s = 54.8$ barg	7.3 mm	7.3 mm	7.3 mm
FE-CFD	~11.5 mm	~10.7 mm	~10.0 mm

5. NUMERICAL ANALYSES

5.1 Numerical modelling approach

The numerical models applied in this study are based on the 'SINTEF coupled FE-CFD model'. The FE-CFD modelling approach is outlined in this document; more details are found in [17, 18, 24]. The FE-CFD model is built within the framework of the commercial finite element (FE) software LS-DYNA [25]. The depressurization upstream of the crack-tip and the pressure of the escaping fluid downstream of the crack-tip are calculated by an in-house computational fluid dynamics (CFD) solver that is coupled with LS-DYNA though a user defined load routine.

The steel pipe is discretized by shell elements. The constitutive model is a rate-dependent J2 formulation applied in combination with the Voce hardening curve, while onset of fracture is modelled by the Cockcroft-Latham (CL) criterion. The flow stress is defined as

$$\sigma_f = \left[\sigma_0 + \sum_{i=1}^{n} Q_i\left(1-\exp\left(-\frac{\theta_i}{Q_i}p\right)\right)\right]\left(1-\frac{\dot{p}}{\dot{p}_0}\right)^c\left[1-\left(\frac{T-T_0}{T_0-T_m}\right)^m\right] \quad (8)$$

where $\dot{p}$ is the equivalent plastic strain-rate, and p is the equivalent plastic strain. Further, σ_0 is the initial yield stress, Q_i and C_i are parameters governing the work hardening, whereas c

and $\dot{p}_0$ are parameters controlling the rate sensitivity. The material temperature is given by T, while T_0 is the reference temperature, T_m is the melting temperature and m is an exponent controlling the temperature influence on the flow stress. Adiabatic heating is included, and the Taylor-Quinney coefficient is set to 0.9 implying that 90% of the plastic work is converted to heat. The CL fracture criterion is expressed as:

$$W = \int_0^p \langle \sigma_I \rangle dp \le W_C, \quad \langle \sigma_I \rangle = \max(\sigma_I, 0) \tag{9}$$

where W_C is the fracture parameter and σ_I is the major principal stress. As W_C is reached in one integration point, the element loses its deviatoric strength. The propagating crack is thus treated as a series of fracture initiations in the elements along the crack path. The fracture criterion is only applied in a seam of elements located at the 12 o'clock position along the pipe length. It is commonly observed that in running ductile fracture scenarios, ring-off is typically followed by immediate arrest. Thus, excluding ring-off in the simulations is considered conservative.

The one-dimensional fluid model calculates two pressures at each axial computational cell: the cross-sectional average pressure p_{av}, and the escape pressure p_e. The latter is only calculated downstream of the crack-tip. To calculate p_{av} and p_e, a homogeneous equilibrium model is employed. It is assumed that the phases have the same temperature, pressure, chemical potential and velocity, thus the governing equations will have the same form as the Euler equations for single-phase compressible inviscid flow. The thermodynamic properties of the mixture are calculated using the Span-Wagner EOS [20]. For the fluid behavior ahead of the propagating crack tip, the average pressure, p_{av}, is applied to all shell elements corresponding to each fluid computational cell. Behind the crack tip, the circumferential pressure variation is modelled using a pressure-profile reconstruction. The outflow is calculated as quasi-steady isentropic compressible Bernoulli flow in a variable cross-section. Because the flow is assumed to be steady and adiabatic, a simple form of choked flow theory is employed, which states that the escape velocity cannot exceed the local speed of sound at the point of escape. More details on the CFD model and the pressure-profile reconstruction are found in [17].

5.2 Project specific FE-CFD models

A pipe-segment with a length of 5 m is modelled in this study, see FIGURE 6, where a symmetry boundary condition in the longitudinal direction is applied on the side of fracture initiation. The length of the half-pipe corresponds to 15.4 × OD which should be sufficient to represent a steady-state crack velocity in a pipe where arrest does not occur. At the end of the pipe on the right-hand side in FIGURE 6, a non-reflecting boundary condition (BC) is applied in the CFD model, thus no reflecting decompression wave will interfere with the propagating crack. The end of the pipe is fixed to ensure stability in the FE solver. The pipe is discretized by Belytschko-Tsai shell elements (LS-DYNA type 2) with five integration points over the thickness. At the 12 o'clock position, a seam of shell elements is located, where the crack is allowed to propagate. The shell elements along the crack seam have an initial length equal to the wall thickness, t, in the longitudinal direction and an initial length of $t/2$ in the hoop direction. Since most of the deformation occurs in the hoop direction, the aspect ratio is near unity at element failure, see [18]. The element size is chosen to capture the local necking that occurs in front of the crack-tip. The length scale of the local neck is in the vicinity of the wall thickness, more details are given in [18]. The model is not supported by soil or water, which is conservative with respect to crack arrest. However, a rigid wall is positioned 50 mm below the bottom of the pipe, thus preventing the pipe from exaggerated deformation in the downward direction. The initial pressure loading from the fluid is gradually applied to the pipe walls over a 6 ms period in a loading step where the implicit solver of LS-DYNA is used, see [24] and [26]. There then follows a rupture step which applies the explicit solver. At the beginning of the rupture step, a line of elements at the crack seam is deleted simultaneously to represent an initial crack. The length of the initial crack is conservatively set to 3×OD = 972 mm, see FIGURE 6. This ensures a large opening effect in the simulation, i.e. the initial pressure works on a large area providing an initial crack-driving force that is larger than what can be expected in a real situation.

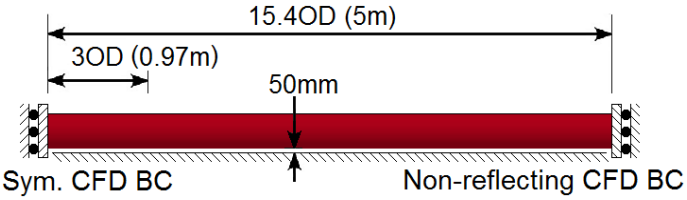

FIGURE 6: FE-CFD MODEL AND BOUNDARY CONDITIONS

The applied load in the simulations is the highest estimated load, i.e. load case I from FIGURE 5 with an initial pressure of 57 bar and a saturation pressure of 55.8 bar. Several models are built to estimate the minimum thickness needed to arrest a crack for each of the three toughness values: 100 J, 125 J and 200 J.

5.3 Calibration of steel material model

For the yield stress and the work hardening properties, a representative curve for a typical L450 pipe was sought. For the FE-CFD model it is not important if this curve stems from an HFW or seamless pipe, analogous to the role of the flow stress, σ_f, in the TCM analysis. It was chosen to apply the work hardening from a 12" HFW 450 PD line pipe used for the Gullfaks Rimfaksdalen project. FIGURE 7 shows the true stress-true plastic strain curve and the fitted Voce hardening curve, and the work hardening parameters of the Voce model. The strain-rate parameters from a previous study on a grade X65 steel [24] are applied in the model; $c = 0.011$ and $\dot{p}_0 = 0.015\ \mathrm{s}^{-1}$. The reference temperature at which the yield stress is defined is $T_0 = 293$ K, the steel melting temperature is set to $T_m = 1800$ K and the temperature sensitivity of the flow stress is assumed to be linear, i.e. $m = 1$, which is consistent with the modelling assumptions found in several other studies on steels, e.g. [27, 28].

The calibration of the Cockcroft-Latham fracture parameter follows the same methodology as in [18]. First, simulations of a full-size Charpy V-notch test are run with 0.3 mm solid elements to establish a fracture parameter for small solid elements, W_C^{solid}, for each C_V value. Scaling is then performed to obtain a fracture parameter representing the length scale of the crack-seam shell-elements in the burst test simulations (t/2 in the hoop direction). In the FE-CFD simulations we want to investigate the effect of wall thickness (t), and so the scaling procedure is carried out for wall thicknesses of 7, 10, 12.9 and 15.9 mm. The scaling was performed by simulating a uniaxial tension test for each thickness, t, using small solid elements. In the simulation the resulting displacements, as measured from a virtual extensometer with gauge length of t/2, were then collected up to the time corresponding to onset of fracture (defined by W_C^{solid}). The collected displacements were then applied as uniaxial tensile loading in a new simulation of a quadrilateral shell element with initial dimensions of $t/2 \times t/2$ and a thickness of t. From the histories of the major principal stress and the equivalent plastic strain, the W_C^{shell} value was established by invoking Eq. (9). The resulting W_C^{shell} parameter that relates to each of the three C_V values for t=[7, 10, 12.9, 15.9] mm are given in FIGURE 8. As expected, the W_C^{shell} value decreases for larger length-scale and increases for higher C_V values. More details on the fracture calibration procedure can be found in [18].

σ_0	θ_1	Q_1	θ_2	Q_2	θ_3	Q_3
450	1040	165.8	13937	80.5	250	25000

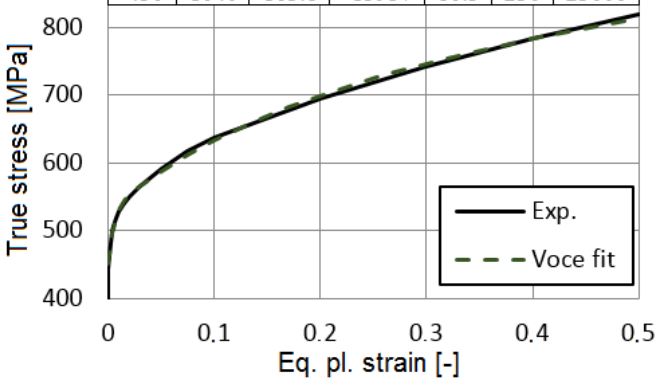

FIGURE 7: EXPERIMENTAL AND VOCE FITTED TRUE STRESS VERSUS TRUE PLASTIC STRAIN. THE VOCE PARAMETERS ARE TABULATED IN MEGAPASCAL

5.4 Numerical results

The results from a total of 12 FE-CFD simulations are given in this section: simulations with four wall thicknesses for each C_V value. In most simulations, the applied W_C^{shell} value was established by interpolation of the values given in FIGURE 8. The final deformation from simulation models based on $C_V = 200$ J is given in FIGURE 9. In the case t=15.9 mm, the crack arrests after 0.7 m of propagation, while for t=10.25 mm, the crack arrests after 2.7 m of propagation. In the t=9.75 mm case, the simulation stops when the crack is 1 × OD (0.32 m) from the right-hand edge of the pipe due to a built-in criterion in the solver. The last 1-2 × OD (0.32-0.65 m) of the crack path in this simulation could be influenced by the fixed BC on the right-hand side. As can be seen from FIGURE 10, the crack has a high and relatively steady velocity after 10 × OD (3.2 m) propagation, thus this simulation is considered as a crack propagation case. The minimum wall thickness to arrest a crack for $C_V = 200$ J is then between 9.75 mm and 10.25 mm. Similarly, the required wall thickness for crack arrest is between 11.25 mm and 11.75 mm for $C_V = 100$ J, and between 10.5 mm and 11.0 mm for $C_V = 125$ J. From the crack velocity curves in FIGURE 10 it can be seen that the crack velocity steadily increases until a maximum velocity lying between 170 m/s and 180 m/s is reached after ~2 × OD (0.65 m). Then the velocity drops until it reaches a local minimum at ~7 × OD (2.3 m). In the case where the crack does not arrest, this minimum is followed by a steady-state velocity. In some of the cases where the crack does arrest (200 J–10.25 mm and 125 J–11.00 mm) the local minimum is followed by a small plateau before arrest. It appears that the lower bound of the steady-state velocity is approximately 75 m/s.

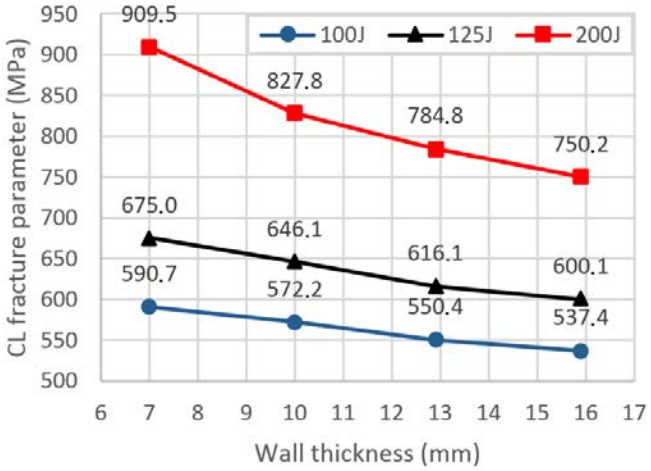

FIGURE 8: W_C^{shell} VALUES AS FUNCTION OF WALL THICKNESS FOR THREE CHARPY V-NOTCH VALUES

TABLE 3 summarizes the approximate minimum wall thickness, $t_{\min}$, needed to arrest a propagating crack from the FE-CFD simulations and the TCM analyses. It can be seen that the TCM analysis with safety factors $\gamma_{sat} = 1.3$ and $\gamma_{CO2} = 1.2$ produces a similar $t_{\min}$ as the FE-CFD simulation for $C_V = 200$ J. However, while the minimum wall thickness in the TCM analysis is insensitive to the C_V value, the FE-CFD analyses produce a significant increase in $t_{\min}$ for decreasing C_V values.

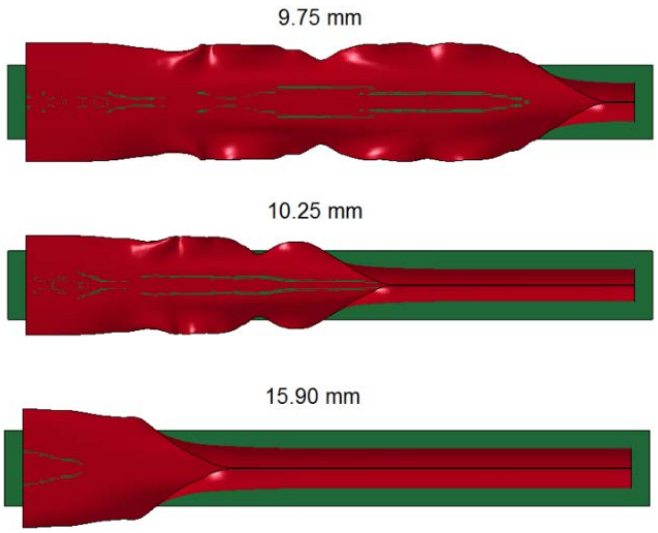

FIGURE 9: RESULTS FROM SIMULATIONS BASED ON $C_V = 200$ J. FINAL DEFORMATION IN SIMULAITONS WITH 9.75 mm, 10.25 mm AND 15.9 mm WALL THICKNESS. THE LATTER TWO ARE AT CRACK ARREST, WHILE THE FORMER IS STOPPED BY A USER DEFINED CRITERION

6. DISCUSSION

If the pipe is backfilled with soil or submerged under water, this will give additional resistance to crack propagation arising from two factors: first, the increased ambient pressure outside the pipe reduces the effective pressure that drives the crack forward; and second, the inertial forces from the mass accelerated by the flaring walls downstream of the crack will work against the crack driving pressure. Four additional simulations are run based on the $C_V = 200$ J pipe material and with wall thickness reduced to 9 mm. One simulation has the same BC as in the previous section, while in the second simulation the pipe is on the seabed. In the third simulation the pipe is backfilled, while in the fourth the pipe is trenched. The three new boundary conditions for the pipe are shown in FIGURE 11. The soil material is modelled by the *MAT_MOHR_COULOMB model in LS-DYNA [25] with the parameters for silt presented in [18]. The water is modelled by the *EOS_GRUNEISEN model [25] with the input parameters from [29] and [30]. The input parameters for these two models are compiled in TABLE 4. The distance between the SPH particles is set to 50 mm and a penalty-based contact formulation with a Coulomb friction coefficient of 0.4 is applied between the smoothed particle hydrodynamics (SPH) particles and the pipe. The hydrostatic pressure / earth pressure from the water / soil is not included in the simulation, i.e. only the effect of shear deformation / inertia adds resistance to the propagating crack. As can be seen from FIGURE 12, the simulation without backfill has a steady-state crack propagation of ~140 m/s while the introduction of water or soil around the pipe leads to rapid crack arrest. In the trenched simulation, the crack velocity increases to ~140 m/s before the flaring pipe walls meet the soil and the crack is arrested. The seabed simulation has a slightly larger final crack-length. The density, and therefore the inertia, of the water is lower than that of the soil. On the other hand, the viscous forces from water should add significant resistance. Since the viscous forces increase with crack velocity, it could be that the effect of the seabed boundary condition is larger for a propagating crack. It is emphasized that the modelling of soil and water needs more attention to give accurate predictions, however, the present results underline the conservativism in designing the pipe without considering the effects of soil or water.

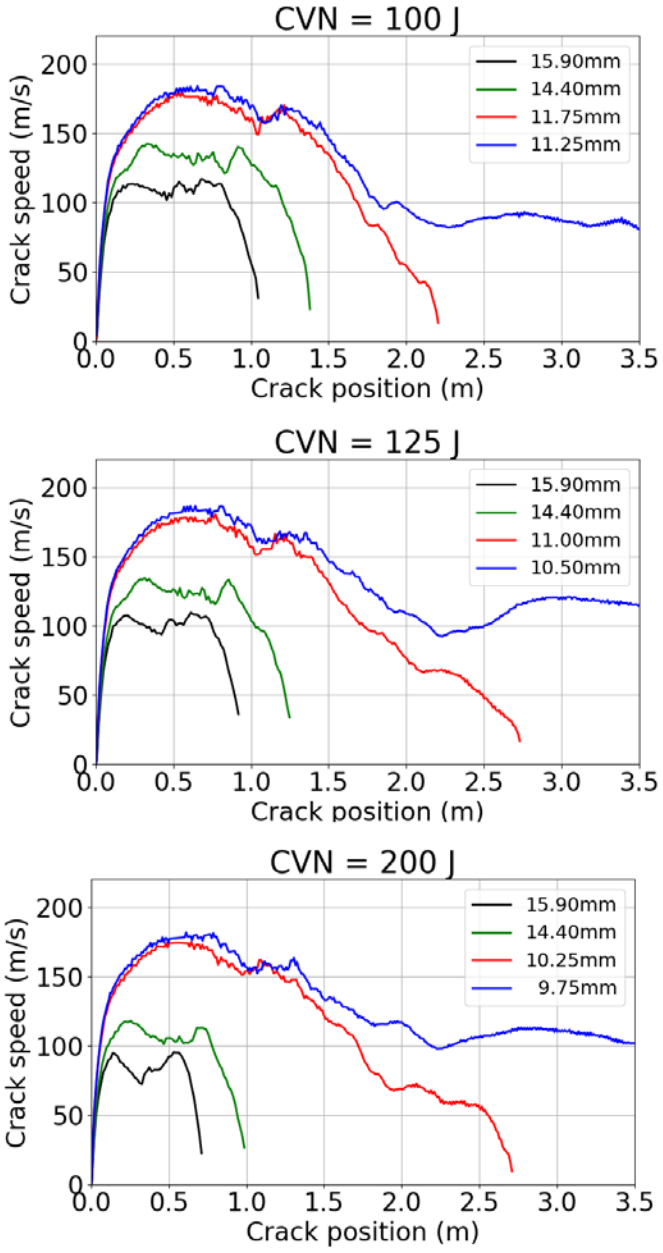

FIGURE 10: CRACK VELOCITY AS FUNCTION OF CRACK LENGTH IN SIMULATIONS WITH VARIOUS CHARPY V-NOTCH VALUES (CVN) AND WALL THICKNESS

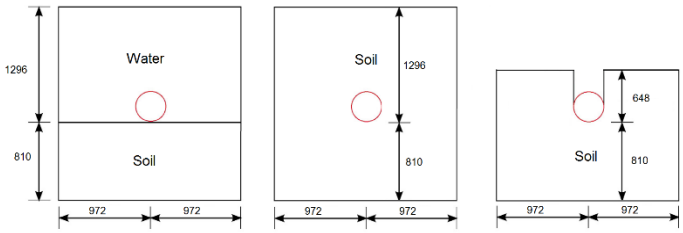

FIGURE 11: SEABED, BACKFILL AND TRENCHED BOUNDARY CONDITIONS FOR THE PIPE

TABLE 4: INPUT PARAMETERS FOR THE MOHR-COULOMB CONSTITUTIVE MODEL FOR SILT [18] AND THE GRÜNEISEN EOS FOR WATER [29, 30]

Mohr-Coulomb parameters					
ρ[kg/m^3]	G [MPa]	ν	ϕ	C [kPa]	ψ
1750	14.8	0.25	35^0	2	5^0
Grüneisen parameters					
P [kg/m^3]	C_0 [m/s]	S_1	S_2	S_3	-
1025	1480	2.56	−1.986	1.2268	-

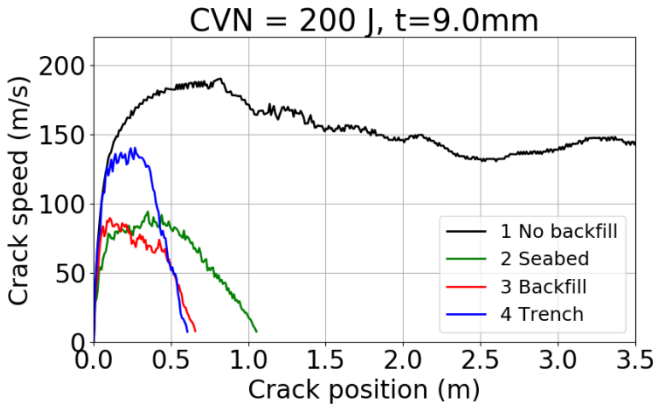

FIGURE 12: CRACK VELOCITY FOR PIPE WITH 9.0 mm WALL THICKNESS AND CHARPY V-NOTCH VALUE OF 200 J, AND PIPE WITH DIFFERENT BOUNDARY CONDITIONS

In the numerical analyses of Section 5.4, the effect of backfill is excluded from the FE-CFD model, and a conservative estimate of the applied loading is used with a saturation pressure of 55.8 bar. The minimum wall thickness, $t_{\min}$, from the numerical analyses stems from the TCM analyses with the DNV-GL RP-F104 safety factors $\gamma_{CO2} = 1.2$ and $\gamma_{sat} = 1.3$, i.e. the minimum wall thickness to ensure crack arrest is estimated as ~10 mm. For comparison, the CO2PIPETRANS test 2 [17] was conducted for a pipe with similar mechanical properties as the ones used in the present study (YS=454 MPa, TS=578 MPa and $C_V = 121$ J), but with a 23 % larger diameter (400 mm). Here, a wall thickness of 6.1 mm (OD/t=66) was sufficient to provide crack arrest in the case of CO_2 loading from a saturation pressure of 39 bar. Compared to the result from this test and given the conservative measures in the numerical and TCM analyses, the estimated $t_{\min}$ of ~10 mm (OD/t=32) is deemed conservative.

7. CONCLUSIONS

The proposed pipeline dimensions for the Northern Lights full-scale CO_2 project have been assessed with respect to running-ductile fracture. The main conclusion is that, for the given pipe material and diameter, and the given loading conditions, a wall thickness of 15.9 mm, or even a wall thickness of 14.3 mm accounting for a lower selected wall thickness for installation, is sufficient for arresting a propagating crack. The TCM with appropriate DNVGL RP-F104 arrest pressure corrections is also shown to be capable of providing a good first estimate in pipe design. However, a result of this study is that the arrest pressure saturates for low CVN values – an observation indicative of limited accuracy.

ACKNOWLEDGEMENTS

The work has been funded by Equinor, its partners and Gassnova through the Northern Lights project. The support from the Norwegian CCS Research Centre, Centre for Environment-friendly Energy Research (Research Council of Norway 257579), is gratefully acknowledged.

REFERENCES

[1] Maxey, W.A. (1974) Fracture Initiation, Propagation and Arrest in 5th Symposium on Line Pipe Research: Huston, Texas.
[2] Cosham, A., Jones, D.G., Armstrong, K., Allason, D. and Barnett, J. (2012) Ruptures in Gas Pipelines, Liquid Pipelines and Dense Phase Carbon Dioxide Pipelines. ASME 9th International Pipeline Conference, Paper IPC2012-90463, Calgary Canada .
[3] A., M.W. (1986) Long Shear Fractures in CO2 Lines Controlled by Regulating Saturation Arrest Pressures. Oil and Gas Journal, **84**(31): p. 44-46.
[4] DNV-GL (2017) DNVGL-RP-F104 Design and operation of CO2 pipelines.
[5] ISO/TC 265 (2016) ISO 27913:2016 Carbon dioxide capture, transportation and geological storage -Pipeline transportation systems.
[6] Cosham, A., Jones, D.G., Armstrong, K., Allason, D. and Barnett, J. (2014) Analysis of two dense phase carbon dioxide full-scale fracture propagation tests. ASME 10th International Pipeline Conference, Paper IPC2014-33080, Calgary, Canada.
[7] Cosham, A., Jones, D.G., Armstrong, K., Allason, D. and Barnett, J. (2016) Analysis of a Dense Phase Carbon Dioxide Full-Scale Fracture Propagation Test in 24 Inch Diameter Pipe. ASME 11th International Pipeline Conference, Paper IPC2016-64456, Calgary, Canada.
[8] Di Biagio, M., Lucci, A., Mecozzi, E. and Spinelli, C.M. (2017) Fracture Propagation Prevention on CO2 pipelines: Full Scale Experimental Testing and Verification Approach in Pipeline Technology Conference 2017: Berlin.

[9] Michal, G., Davis, B., Østby, E., Lu, C. and Røneid, S. (2018) CO2SAFE-ARREST: A Full-Scale Burst Test Research Program for Carbon Dioxide Pipelines — Part 2: Is the BTCM Out of Touch With Dense-Phase CO2? ASME 12th International Pipeline Conference, Paper IPC2018-78525, Calgary, Canada.
[10] O'Donoghue, P.E., Kanninen, M.F., Leung, C.P., Demofonti, G. and Venzi, S. (1997) The development and validation of a dynamic fracture propagation model for gas transmission pipelines. International Journal of Pressure Vessels and Piping, **70**(1): p. 11-25.
[11] Shim, D.-J., Wilkowski, G., Rudland, D., Rothwell, B. and Merritt, J. (2008) Numerical Simulation of Dynamic Ductile Fracture Propagation Using Cohesive Zone Modeling. ASME 7th International Pipeline Conference, Calgary, Canada
[12] Nakai, H., Shibanuma, K. and Aihara, S. (2016) Numerical model for unstable ductile crack propagation and arrest in pipelines using finite difference method. Engineering Fracture Mechanics, **162**: p. 179-192.
[13] Botros, K.K., Clavelle, E.J., Uddin, M., Wilkowski, G. and Guan, C. (2018) Next Generation Ductile Fracture Arrest Analyses for High Energy Pipelines Based on Detail Coupling of CFD and FEA Approach. ASME 12th International Pipeline Conference, Paper IPC2018-78097, Calgary, Canada.
[14] Mahgerefteh, H., Brown, S. and Denton, G. Modelling the impact of stream impurities on ductile fractures in CO2 pipelines. Chemical Engineering Science, **74**: 200–210.
[15] Keim, V., Marx, P., Nonn, A. and Münstermann, S. (2019) Fluid-structure-interaction modeling of dynamic fracture propagation in pipelines transporting natural gases and CO2-mixtures. International Journal of Pressure Vessels and Piping, **175**: p. 103934.
[16] Keim, V., Paredes, M., Nonn, A. and Münstermann, S. (2020) FSI-simulation of ductile fracture propagation and arrest in pipelines: Comparison with existing data of full-scale burst tests. International Journal of Pressure Vessels and Piping, **182**: p. 104067.
[17] Aursand, E., Dumoulin, S., Hammer, M., Lange, H.I., Morin, A., Munkejord, S.T. and Nordhagen, H.O. (2016) Fracture propagation control in CO2 pipelines: Validation of a coupled fluid–structure model. Engineering Structures, **123**: p. 192-212.
[18] Nordhagen, H.O., Munkejord, S.T., Hammer, M., Gruben, G., Fourmeau, M. and Dumoulin, S. (2017) A fracture-propagation-control model for pipelines transporting CO2-rich mixtures including a new method for material-model calibration. Engineering Structures, **143**(Supplement C): p. 245-260.
[19] Gruben, G., Dumoulin, S., Nordhagen, H., Hammer, M. and Munkejord, S.T. (2018) Simulation of a Full-Scale CO2 Fracture Propagation Test. ASME 12th International Pipeline Conference, Calgary, Canada.
[20] Span, R. and Wagner, W. (1996) A New Equation of State for Carbon Dioxide Covering the Fluid Region from the Triple-Point Temperature to 1100 K at Pressures up to 800 MPa. Journal of Physical and Chemical Reference Data, **25**(6): p. 1509-1596.
[21] Leis, B. (2015) Arresting propagating shear in pipelines. Steel in Translation, **45**(1): p. 1-17.
[22] Wilkowski, G., Maxey, W. and Eiber, R. (1977) Use of a brittle notch DWTT specimen to predict fracture characteristics of line pipe steels. in ASME 1977 Energy Technology Conference, Houston, Texas, Paper.
[23] Cosham, A., Jones, D., Leis, B., Hopkins, P. and Barnett, J. (2013) Not another Charpy V-Notch correction factor...? in Proceedings of the 6th International Pipeline Technology Conference, Paper.
[24] Nordhagen, H.O., Kragset, S., Berstad, T., Morin, A., Dørum, C. and Munkejord, S.T. (2012) A new coupled fluid–structure modeling methodology for running ductile fracture. Computers & Structures, **94-95**(Supplement C): p. 13-21.
[25] LSTC (2015) LS-DYNA KEYWORD USER'S MANUAL in LS-DYNA R8.0 03/23/15 (r:6319). Livermore Software Technology Corporation: Livermore, California 94551-0712.
[26] Uddin, M. and Wilkowski, G. (2016) Simulation of Dynamic Crack Propagation and Arrest Using Various Types of Crack Arrestor. ASME 11th International Pipeline Conference, Paper IPC2016-64561, Calgary, Canada.
[27] Børvik, T., Hopperstad, O.S., Berstad, T. and Langseth, M. (2001) A computational model of viscoplasticity and ductile damage for impact and penetration. European Journal of Mechanics - A/Solids, **20**(5): p. 685-712.
[28] Børvik, T., Dey, S. and Clausen, A.H. (2009) Perforation resistance of five different high-strength steel plates subjected to small-arms projectiles. International Journal of Impact Engineering, **36**(7): p. 948-964.
[29] Steinberg, D.J. (1987) Spherical explosions and the equation of state of water. Lawrence Livermore National Laboratory. Report UCID-20974
[30] Shin, Y.S., Lee, M., Lam, K.Y. and Yeo, K.S. (1998) Modeling Mitigation Effects of Watershield on Shock Waves. Shock and Vibration 5(4):225-234.